J|A|C|S
ARTICLES
Published on Web 04/27/2004

Electrochemistry and Optical Absorbance and Luminescence of Molecule-like Au_{38} Nanoparticles

Dongil Lee,† Robert L. Donkers,‡ Gangli Wang, Amanda S. Harper, and Royce W. Murray*

Contribution from the Kenan Laboratories of Chemistry, University of North Carolina, Chapel Hill, North Carolina 27599

Received January 22, 2004; E-mail: rwm@email.unc.edu

Abstract: This paper describes electrochemical and spectroscopic properties of a well-characterized, synthetically accessible, 1.1 nm diam Au nanoparticle, $Au_{38}(PhC_2S)_{24}$, where PhC_2S is phenylethylthiolate. Properties of other Au_{38} nanoparticles made by exchanging the monolayer ligands with different thiolate ligands are also described. Voltammetry of the Au_{38} nanoparticles in CH_2Cl_2 reveals a 1.62 V energy gap between the first one-electron oxidation and the first reduction. Based on a charging energy correction of ca. 0.29 V, the indicated HOMO−LUMO gap energy is ca. 1.33 eV. At low energies, the optical absorbance spectrum includes peaks at 675 nm (1.84 eV) and 770 nm (1.61 eV) and an absorbance edge at ca. 1.33 eV that gives an optical HOMO−LUMO gap energy that is consistent with the electrochemical estimate. The absorbance at lowest energy is bleached upon electrochemical depletion of the HOMO level. The complete voltammetry contains two separated doublets of oxidation waves, indicating two distinct molecular orbitals, and two reduction steps. The ligand-exchanged nanoparticle $Au_{38}(PEG_{135}S)_{13}(PhC_2S)_{11}$, where $PEG_{135}S$ is $-SCH_2CH_2OCH_2CH_2OCH_3$, exhibits a broad (1.77−0.89 eV) near-IR photoluminescence band resolvable into maxima at 902 nm (1.38 eV) and 1025 nm (1.2 eV). Much of the photoluminescence occurs at energies less than the HOMO−LUMO gap energy. A working model of the energy level structure of the Au_{38} nanoparticle is presented.

Introduction

Gold nanoparticles have received much attention owing to their novel optical and electronic properties and potential optical and chemical sensing applications.[1] Au nanoparticles containing <200 down to a few tens of atoms are of special interest because they encompass the transition between bulk and molecular regimes, where electronic band energetics yield to quantum confinement effects, and discrete electronic states emerge. Two key issues in the study of such very small nanoparticles are property dependence on nanoparticle size and on the capping or protecting ligands bonded to the nanoparticle surface. Size and ligand dependence are interrelated, since the fraction of atoms of the nanoparticle that are ligand-bonded increases as size decreases. The quantum size confinement is manifested as property changes that bring out molecule-like forms of behavior.[2,3]

This paper describes properties of a purified molecule-like, monolayer-protected Au_{38} nanoparticle. Molecule-like nanoparticles have been previously isolated using fractional precipitation and chromatographic fractionation.[4,5] A size-dependent opening of a HOMO−LUMO (the highest occupied and lowest unoccupied molecular orbitals) energy gap, representing the bulk-to-molecule transition,[3c] has been reported based on voltammetric and near-IR studies of alkanethiolate-coated monolayer-protected metal clusters (MPCs) with Au core masses of 8 to 38 kDa. Recently, Hutchison and co-workers[6] prepared alkanethiolate-protected Au_{11} by replacing the triphenylphos-

† Present address: Department of Chemistry, Western Michigan University, Kalamazoo, MI 49008-5413.

‡ Present address: Steacie Institute for Molecular Sciences, National Research Council of Canada, Ottawa, Ontario, K1A 0R6, Canada.

(1) (a) Hayat, M. A., Ed. *Colloidal Gold: Principles, Methods, and Applications*; Academic Press: San Diego, CA, 1991. (b) Wood, A.; Giersig, M.; Mulvaney, P. *J. Phys. Chem. B* **2001**, *105*, 8810−8815. (c) Sampaio, J. F.; Beverly, K. C.; Heath, J. R. *J. Phys. Chem. B* **2001**, *105*, 8797−8800. (d) Vance, F. W.; Lemon, B. I.; Hupp, J. T. *J. Phys. Chem. B* **1998**, *102*, 10091−10093. (e) Feldheim, D. L.; Keating, C. D. *Chem. Soc. Rev.* **1998**, *27*, 1−12. (f) Zanchet, D. M.; Micheel, C. M.; Parak, W. J.; Gerion, D.; Alivisatos, A. P. *NanoLett.* **2001**, *1*, 32−35. (g) Nam, J.-M.; Thaxton, C. S.; Mirkin, C. A. *Science* **2003**, *301*, 1884−1886. (h) Elghanian, R.; Storhoff, J. J.; Mucic, R. C.; Letsinger, R. L.; Mirkin, C. A. *Science* **1997**, *277*, 1078−1080. (i) Templeton, A. C.; Wuelfing, W. P.; Murray, R. W. *Acc. Chem. Res.* **2000**, *33*, 27−36.

(2) (a) Alivisatos, A. P. Science, **1996**, *271*, 933. (b) Brus, L. E. *J. Phys. Chem.* **1986**, *90*, 2555. (c) Heath, J. R. *Science* **1995**, *270*, 1315. (d) Murray, C. B.; Kagan, C. R.; Bawendi, M. G. *Science* **1995**, *270*, 1335.

(3) (a) Link, S.; Beeby, A.; FitzGerald, S.; El-Sayed, M. A.; Schaaff, T. G.; Whetten, R. L. *J. Phys. Chem. B* **2002**, *106*, 3410−3415. (b) Schaaff, T. G.; Knight, G.; Shafigullin, M. N.; Borkman, R. F.; Whetten, R. L. *J. Phys. Chem. B* **1998**, *102*, 10643−10646. (c) Chen, S.; Ingram, R. S.; Hostetler, M. J.; Pietron, J. J.; Murray, R. W.; Schaaff, T. G.; Khoury, J. T.; Alvarez, M. M.; Whetten, R. L. *Science* **1998**, *280*, 2098−2101.

(4) (a) Schaaff, T. G.; Shafigullin, M. N.; Khoury, J. T.; Vezmar, I.; Whetten, R. L.; Cullen, W. G.; First, P. N.; Gutiérrez-Wing, C.; Ascensio, J.; Jose-Yacamán, M. J. *J. Phys. Chem. B* **1997**, *101*, 7885. (b) Whetten, R. L.; Khoury, J. T.; Alvarez, M. M.; Murthy, S.; Vezmar, I.; Wang, Z. L.; Stephens, P. W.; Cleveland, C. L.; Luedtke, W. D.; Landman, U. *Adv. Mater.* **1996**, *8*, 428−433.

(5) (a) Jimenez, V. L.; Leopold, M. C.; Mazzitelli, C.; Jorgenson, J. W.; Murray, R. W. *Anal. Chem.* **2003**, *75*, 199. (b) Wei, G.; Liu, F.; Wang, C. R. C. *Anal. Chem.* **1999**, *71*, 2085−2091. (c) Wilcoxon, J. P.; Martin, J. E.; Provencio, P. *Langmuir* **2000**, *16*, 9912−9920. (d) Schnabel, U.; Fischer, C.; Kenndler, E. *J. Microcolumn Sep.* **1997**, *9*, 529−534. (e) Templeton, A. C.; Cliffel, D. E.; Murray, R. W. *J. Am. Chem. Soc.* **1999**, *121*, 7081−7089.

(6) Woehrle, G. H.; Warner, M. G.; Hutchison, J. E. *J. Phys. Chem. B.* **2002**, *106*, 9979.

phine ligands of a preformed Au_{11} core. In related work, Yang and Chen[7] reported that the Au_{11} nanoparticle's HOMO−LUMO gap increases from 1.4 to 1.8 eV (from voltammetry and absorbance spectra) upon replacement of the initial triphenylphosphines with dodecanethiolate ligands. Quinn and coworkers[8] report a hexanethiolate-coated nanoparticle assigned (without analytical evidence) as having a Au_{38} core and exhibiting a 1.2 eV gap between the first voltammetric oxidation and the first reduction.

The molecule-like phenylethanethiolate-protected Au_{38} cluster (Au_{38} MPC) described here was isolated based on a strong solubility differentiation from larger nanoparticles.[9] The focus of this paper is its spectroscopic and electrochemical charging properties; its synthesis and isolation and a thorough analytical confirmation have been presented earlier.[9] Ligand-exchanged variants of this nanoparticle, $Au_{38}(PEG_{135}S)_{13}(PhC_2S)_{11}$, $Au_{38}(C_6S)_{22}(PhC_2S)_2$, and $Au_{38}(C_{10}S)_{19}(PhC_2S)_5$, where $PEG_{135}S-$ is $-SCH_2CH_2OCH_2CH_2OCH_3$, C_6S- is hexanethiolate, and $C_{10}S-$ is decanethiolate, respectively, are also described. The electrochemical formal potentials for the first one-electron reduction and one-electron oxidation of $Au_{38}(PhC_2S)_{24}$ and its ligand exchanged variants are separated by 1.65(±0.03) V, with minor dependencies on ligand, solvent, and temperature. The large electrochemical potential spacing is consistent with a molecule-like, discretized electronic energy level structure for these Au_{38} MPCs. Correction of the electrochemical energy gap for charging energy (also called[10] "addition energy") as described later gives an HOMO−LUMO gap energy somewhat above 1.3 eV, which corresponds very well to the observed ca. 1.33 eV optical absorption onset of $Au_{38}(PhC_2S)_{24}$. The consistency of electrochemical with optical HOMO−LUMO gap energies is supported by spectroelectrochemistry showing a partial bleach of the low energy optical absorbance upon oxidation of the Au_{38} MPC and depletion of the HOMO level.

A number of electrochemical oxidation and reduction steps are observable below and above, respectively, the initial oxidation and reduction reactions of $Au_{38}(PhC_2S)_{24}$. These reactions appear as doublet steps of single-electron changes that in the accessible potential range in CH_2Cl_2 lead ultimately to $Au_{38}(PhC_2S)_{24}^{4+}$ and to $Au_{38}(PhC_2S)_{24}^{2-}$. The potential spacing between the doublet of peaks for the $Au_{38}(PhC_2S)_{24}^{+1/0}$ and $Au_{38}(PhC_2S)_{24}^{+2/+1}$ reactions is used to estimate the charging energy for this nanoparticle's reaction.[10]

The ligand-exchanged $Au_{38}(PEG_{135}S)_{13}(PhC_2S)_{11}$ nanoparticle is also photoluminescent, at energies spanning the HOMO−LUMO gap energy.

Experimental Section

Chemicals. 2-Phenylethanethiol (PhC_2SH, 99%), decanethiol (98%), hexanethiol (98%), tetra-*n*-octylammonium bromide (98%), and sodium borohydride (99%) were used as received from Aldrich, as were toluene (Fisher, reagent grade), acetonitrile (Fisher, Optima), methylene chloride (Fisher, reagent grade), and ethanol (Aarper Alcohol and Chemical Company). Hydrogen tetrachloroaurate trihydrate (from 99.999% pure gold) was prepared using a literature procedure[11] and stored in a freezer at −20 °C. Water was purified with a Barnstead NANOpure system (18 MΩ).

Synthesis of $Au_{38}(PhC_2S)_{24}$. $Au_{38}(PhC_2S)_{24}$ was synthesized as described elsewhere.[9] Briefly, in a standard two-phase Brust-style synthesis,[12] hydrogen chloroaurate (3.1 g, 11.1 mmol) was phase-transferred into toluene with tetra-*n*-octylammonium bromide, followed by addition of a 3-fold molar excess (relative to Au) of phenylethanethiol, forming a gold(I)-thiol polymer. This material was reduced by adding a 10-fold excess of aqueous $NaBH_4$ at 0 °C, with vigorous mixing, stirring the product solution at 0 °C for 24 h. After the aqueous layer was removed, the toluene was rotary-evaporated at room temperature. The $Au_{38}(PhC_2S)_{24}$ was extracted from the crude product with acetonitrile and was further purified from tetra-*n*-octylammonium bromide by repeatedly dissolving the crude product in CH_2Cl and reprecipitating with ethanol until only traces of quaternary ammonium cation could be detected (^{1}H NMR). The product was characterized by ^{1}H NMR, UV−vis spectra, and thermogravimetric analysis, as described previously.[9]

Ligand Place-Exchange Reactions. Thiolated poly(ethylene glycol) ($PEG_{135}SH$), decanethiol ($C_{10}SH$), and hexanethiol (C_6SH) were incorporated into the monolayer shell of $Au_{38}(PhC_2S)_{24}$ by ligand exchange.[1i,13] $PEG_{135}SH$ was synthesized as described in the Supporting Information. In a typical procedure, 45 mg of $Au_{38}(PhC_2S)_{24}$ in 5 mL of CH_2Cl_2 were stirred with an excess of ligand for 4 days, the solvent was rotary-evaporated, and the product was rinsed several times with heptane (for $PEG_{135}SH$) or ethanol (for alkanethiols), until the α-thiol proton peak of the free ligand was eliminated from the ^{1}H NMR spectrum. The relative proportions of ligands in the resulting mixed MPC monolayers were assessed by decomposing the MPC with iodine and analyzing the liberated disulfides by ^{1}H NMR.

Electrochemistry. Voltammetry was done with a CHI 660A Electrochemical workstation, in 0.1 M Bu_4NPF_6 solutions that were degassed and blanketed with high-purity Ar atmosphere during the experimental procedure. The working electrode was a 0.4 mm Pt disk, the counter electrode was a Pt wire, and the reference electrode was either a Ag/Ag^+ electrode or a Ag wire quasi-reference electrode, AgQRE. The working electrode was polished with 0.05 μm Al_2O_3 slurries and cleaned electrochemically by potential-cycling in 0.1 M H_2SO_4 solution. Reduced temperature voltammetry was done using cold baths of acetone/dry ice (−70 °C) and acetonitrile/dry ice (−40 °C). Potentials in the tables in this paper are reported vs Ag/Ag^+ which was calibrated as −0.61, −0.64, −0.61, and −0.59 V vs the ferrocene/ferrocenium couple in CH_2Cl_2, 2:1, 1:1, and 1:2 toluene/acetonitrile, respectively (AgQRE). (Irrespective of calibration, *differences* between the potentials of peaks within a given voltammogram are more reliable than actual potentials observed in different voltammograms taken in varied solvents or temperatures. Potential *differences* are reported in the paper; actual potentials are found in the Supporting Information.) Background potential scans in electrolyte solutions were used to check for any spurious peaks.

Spectroscopy. UV−vis spectra were collected with a Shimadzu UV−vis (model UV-1601) spectrometer. Photoluminescence (PL) spectra were taken in a 90° geometry on a modified ISA Fluorolog FL321 spectrometer. The spectrometer is equipped with a 450 W xenon source and Hamamatsu R928 MPT (visible wavelengths) and InGaAs (near-IR wavelengths, connected via a T channel) detectors. Sample solutions were freshly prepared before each measurement.

Spectroelectrochemistry. The quasi-thin layer, demountable spectroelectrochemical cell[14] consisted of two glass slides separated by a

(7) Yang, Y.; Chen, S. *Nano Lett.* **2003**, *3*, 75.
(8) Quinn, B. M.; Liljeroth, P.; Ruiz, V.; Laaksonen, T.; Kontturi, K. *J. Am. Chem. Soc.* **2003**, *125*, 6644.
(9) Donkers, R. L.; Lee. D.; Murray, R. W. *Langmuir* **2004**, *20*, 1945−1952.
(10) (a) Franceschetti, A.; Zunger, A. *Phys. Rev. B* **2000**, *62*, 2614. (b) Creutz, C.; Brunschwig, B. S.; Sutin, N. *Comprehensive Coordination Chemistry II* **2004**, *7*, 731−777.
(11) *Handbook of Preparative Inorganic Chemistry*; Brauer, G., Ed.; Academic Press: New York, 1965; p 1054.
(12) Brust, M.; Walker, M.; Bethell, D.; Schriffrin, D. J.; Whyman, R. *J. Chem. Soc., Chem. Commun.* **1994**, 801.
(13) (a) Hostetler, M. J.; Green, S. J.; Stokes, J. J.; Murray, R. W. *J. Am. Chem. Soc.* **1996**, *118*, 4212. (b) Hostetler, M. J.; Templeton, A. C.; Murray, R. W. *Langmuir* **1999**, *15*, 3782. (c) Song, Y.; Murray, R. W. *J. Am. Chem. Soc.* **2002**, *124*, 7096.

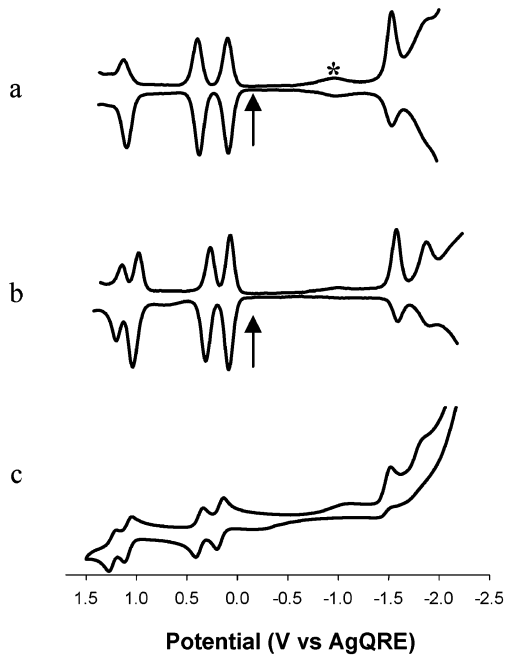

Figure 1. (a) 25 °C and (b) −70 °C differential pulse voltammograms (DPVs) at 0.02 V/s, and (c) −70 °C cyclic voltammogram (0.1 V/s) of $Au_{38}(PhC_2S)_{24}$ in 0.1 M Bu_4NPF_6 in degassed CH_2Cl_2 at 0.4 mm diameter Pt working, Ag wire quasireference (AgQRE), and Pt wire counter electrode. Arrows indicate solution rest potentials, and * indicates wave for incompletely removed O_2, which varied from experiment to experiment.

0.5 mm Teflon spacer, sealed by tightening screws, and enclosing Pt mesh working and Pt wire counter electrodes, and a Ag wire AgQRE. The working and counter electrodes lie side by side, with the beam path masked so that only products of the working electrode are optically monitored. The (air) empty cell provided the reference spectrum, which was subtracted from the results with the filled cell. Initial cyclic voltammograms at 5 mV/s aided determining the appropriate electrolysis potentials, chosen to produce 0, +1, or +2 charge states of the Au_{38} nanoparticles in the degassed, CH_2Cl_2 cell solution. The electrolysis typically required 3 to 5 min for completion (as monitored by current), whereupon a spectrum was taken.

Results and Discussion

Voltammetry, Absorbance Spectra, and Spectroelectrochemistry of CH_2Cl_2 Solutions of $Au_{38}(PhC_2S)_{24}$ Nanoparticles. Figure 1 shows cyclic and differential pulse voltammetry (DPV) of CH_2Cl_2 solutions of $Au_{38}(PhC_2S)_{24}$ nanoparticles. The current peaks in the DPV scans (Figure 1a) lie at the formal potentials of the nanoparticle charge state couples. We see that the formal potentials are unevenly spaced, in contrast to DPV voltammograms[15] of hexanethiolate-coated Au_{140} nanoparticles that display roughly evenly spaced, serial one-electron changes leading ultimately to core charge states as oxidized as Au_{140}^{7+} and as reduced as Au_{140}^{6-}. The latter phenomenon is primarily a quantized double layer (QDL) charging of the MPC cores[15] that is observable at room temperature because of the sub-aF capacitances (C_{CLU}) of MPCs bearing low dielectric monolayer coatings. The electrochemical voltammetry of $Au_{38}(PhC_2S)_{24}$ in Figure 1 is in contrast, qualitatively more like that of large molecular species, such as the fullerenes.[16]

Table 1. Formal Potential[a] Spacings (V) for $Au_{38}(PhC_2S)_{24}$ in Nonaqueous Solvents Containing 0.1 M Bu_4NClO_4

solvent	*T*, °C	ox4–ox3	ox3–ox2	ox2–ox1	ox1–re1	re1–re2	re2–re3	re3–re4
CH_2Cl_2	25		0.73	0.29	1.62			
2:1 tol/MeCN	25		0.64	0.44	1.68	0.24	0.33	0.31
1:1 tol/MeCN	25		0.65	0.32	1.65	0.23	0.25	
1:2 tol/MeCN	25		0.64	0.25	1.60	0.30	0.28	
CH_2Cl_2	−70	0.17	0.72	0.20	1.67	0.31		
2:1 tol/MeCN	−40		0.63	0.38	1.67	0.25	0.24	0.33
1:1 tol/MeCN	−40		0.67	0.30	1.68	0.24	0.29	0.32
1:2 tol/MeCN	−40		0.64	0.22	1.62	0.30	0.27	0.25

[a] Formal potentials are averages of reduction and oxidation peak potentials in the DPV potential scans.

The typical rest potential (Figure 1, arrow) of a solution of the zerovalent ($Au_{38}(PhC_2S)_{24}^0$) form of the nanoparticle is typically about −0.1 V. The electrochemical formal potential for the first one-electron oxidation of $Au_{38}(PhC_2S)_{24}$ is only slightly more positive than this. That the nanoparticle is readily oxidized is consistent with a recent theoretical prediction[17] for $Au_{38}(SCH_3)_{24}$ that filled levels lie just below the Fermi energy. The first *reduction* step of $Au_{38}(PhC_2S)_{24}$ lies, however, at a rather negative potential that is separated from the potential of the first oxidation by an appreciable energy gap of, in CH_2Cl_2 (Figure 1a), 1.62 V. This energy gap contains work terms associated with charging the nanoparticle to Au_{38}^- and Au_{38}^+, the so-called charging or addition energy.[10] This is estimated using the separation between the $Au_{38}^{+/0}$ and $Au_{38}^{2+/1+}$ reaction formal potentials, which from Table 1 (ox2 − ox1) is 0.29 V in CH_2Cl_2. The difference gives a corrected energy of 1.33 eV, which constitutes an electrochemical prediction of the HOMO−LUMO gap energy.

The $Au_{38}^{1+/0}$ and $Au_{38}^{2+/1+}$ reactions are generally well-behaved in terms of chemical reversibility but the other redox reactions display voltammetric symptoms of product instability. The chemical reversibility is improved at lowered temperatures (Figure 1b,c) where the $Au_{38}^{3+/2+}$ wave becomes chemically reversible and the $Au_{38}^{4+/3+}$ reaction becomes nearly so. At room temperature in Figure 1a (and later in Figures 4 and 5), the $Au_{38}^{3+/2+}/Au_{38}^{4+/3+}$ oxidation doublet is not resolved owing to apparent instability of the more highly oxidized forms. The reduction steps are not as well behaved even at lowered temperature, although it is obvious that there are two reduction steps present (and more are seen in other solvents). The first reduction step, at ca. −1.5 V, is partly reversible, and the second reduction, much less so.

The pattern of electrochemical peaks in Figure 1 is two separated doublets of oxidation steps and one of reduction (a second reduction doublet is seen in Figure 5). The doublets are not likely to be caused by the presence of isomers (as found for fullerenes like[16] C_{78}), given the monodispersity evidence from an HPLC experiment.[18] The currents (*) between 0 and −1.5 V vary from experiment to experiment and are attributed to residual oxygen. The potential spacing between current peaks

(14) (a) Heineman, W. R.; O'Dom, G. W.; Murray, R. W. *Anal. Chem*. **1967**, *39*, 1666. (b) Anderson, C. W.; Halsall, H. B.; Heineman, W. R. *Anal. Biochem.* **1979**, *93*, 366.
(15) (a) The roughly even spacing of one-electron changes for Au_{140} on the potential axis implies that C_{CLU}, and the charging energy, is approximately independent of potential. (b) Ingram, R. S.; Hostetler, M. J.; Pietron, J. J.; Murray, R. W.; Schaaff, T. G.; Khoury, J.; Whetten, R. L.; Bigioni, T. P.; Guthrie, D. K.; First, P. N. *J. Am. Chem. Soc.* **1997**, *119*, 9279. (c) Chen, S.; Murray, R. W.; Feldberg, S. W. *J. Phys. Chem. B.* **1998**, *102*, 9898.
(16) (a) Yang, Y.; Arias, F.; Echegoyen, L.; Chibante, L. P. F.; Flanagan, S.; Robertson, A.; Wilson, L. J. *J. Am. Chem. Soc.* **1995**, *117*, 7801. (b) Echegoyen, L.; Echegoyen, L. E. *Acc. Chem. Res.* **1998**, *31*, 593.
(17) Häkkinen, H.; Barnett, R. N.; Landman, U. *Phys. Rev. Lett.* **1999**, *82*, 3264−3267.
(18) Lee, D.; Donkers, R. L.; DeSimone, J. M.; Murray, R. W. *J. Am. Chem. Soc.* **2003**, *125*, 1182.

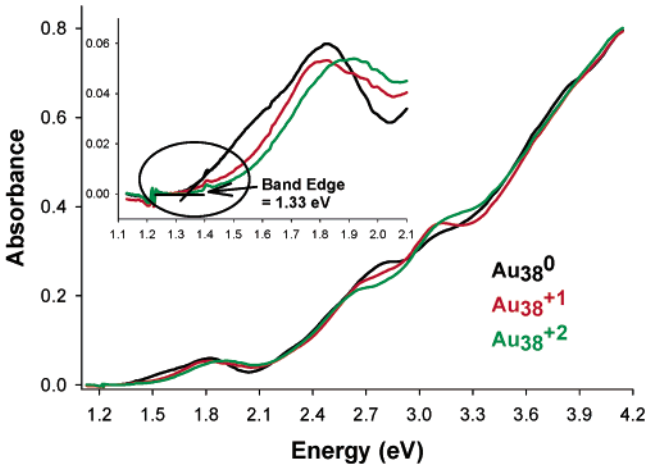

Figure 2. UV−vis spectra (25 °C) of (a) $Au_{38}(PhC_2S)_{24}$ (black line), (b) $Au_{38}(PhC_2S)_{24}^{1+}$(red line), and (c) $Au_{38}(PhC_2S)_{24}^{2+}$ (green line) in degassed CH_2Cl_2 solution. The three spectra are of the same solution; the 1+ and 2+ charge states were generated by electrolysis in the spectroelectrochemical cell. These data are shown in a wavelength axis plot in Figure S-2.

for Figure 1 and other experiments discussed later are listed in Table 1; the actual potentials are given in Table S-1.

The absorbance spectrum (black line) of a CH_2Cl_2 solution of $Au_{38}(PhC_2S)_{24}$ displays (Figure 2), as described before,[18] a steplike structure that is typical for gold MPCs with very small core dimensions.[3] It is instructive to consider the low energy part of this spectrum. The absorbance around 700 nm appears (from fitting to a sum of Gaussians,[19] Figure S-1) to be two overlapping peaks, at 675 nm (1.84 eV) and 770 nm (1.61 eV). Following the absorbance spectrum into the near-infrared, the absorbance appears to be extinguished as an absorbance edge at 1.33 eV, as shown in the Figure 2 inset. This optical band gap energy is identical to the preceding electrochemical estimate of the HOMO−LUMO gap energy for the $Au_{38}(PhC_2S)_{24}$ nanoparticle.

Based on the observations in Figures 1 and 2, we propose, as a rough working model, that the $Au_{38}(PhC_2S)_{24}$ electronic structure contains three well-defined molecular orbitals, two (electron pair occupied) levels below the Fermi level and an empty one above. Each orbital spawns a serial pair of electrochemical reaction steps as electron donors and acceptors. This preliminary orbital diagram model, shown in Figure 3, while very simple, is not unique; Banin et al.,[20] for example, described an analogous state-occupancy diagram based on STS observations of InAs quantum dots.

Besides portraying the HOMO−LUMO gap, Figure 3 also shows a second occupied orbital 0.44 eV below the HOMO. This orbital is predicted by the second oxidation doublet seen in the low-temperature voltammetry in Figure 1b,c. The 0.44 eV energy spacing between the first and second oxidation doublets is based on applying a 0.29 V charging energy correction to the 0.73 V spacing between the two doublets (Table 1, Figure 1). The appearance of the second distinct electronic level below the HOMO signals that the latter is indeed a condensed and discrete electronic level and not merely the edge

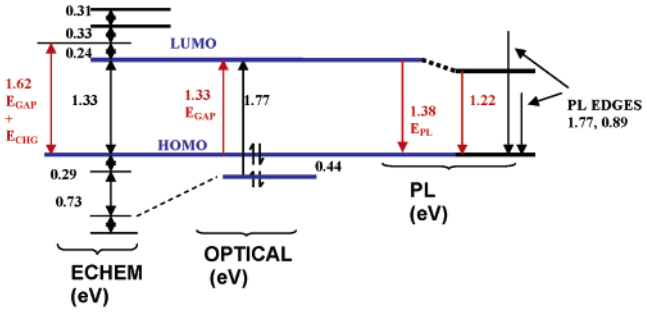

Figure 3. Schematic model energy level diagram for $Au_{38}(PhC_2S)_{24}$, based on data taken in CH_2Cl_2 solution (except for reduction beyond Au_{38}^{1-} where data are from 2:1 toluene/acetonitrile).

of a continuum of electronic states. The energy separation between the lower energy occupied level and the LUMO, 1.77 eV, is near that of the low energy absorbance peak in Figure 2. Finally, the electrochemical changes shown above the LUMO, which have been augmented with data taken in toluene/acetonitrile solution (Table 1), are all roughly equally spaced, by about the same energy as the estimated charging energy. Consequently we cannot identify higher energy orbitals other than the one shown.

The reversible bleaching effect of electrochemical charging in spectra of films of semiconductor quantum dots has been recently reported.[21] For the Au_{38} "quantum dots", if the low energy spectral absorbance (Figure 2) and the electrochemical results (Figure 1) indeed reflect a common energy gap electronic structure, then electrochemically depopulating the HOMO level should attenuate the optical absorbance. The results in Figure 2 were obtained by electrochemical oxidation of Au_{38} nanoparticle solutions in an optically transparent thin layer cell.[14] The Figure 2 inset of the band edge region shows that the spectrum (black line) of $Au_{38}(PhC_2S)_{24}^{0}$ MPCs changes substantially upon oxidation to the Au_{38}^{1+} (red) and Au_{38}^{2+} (green) states. There is a loss in absorbance intensity near the absorbance band edge with an apparent shift in the edge toward higher energy. There are other changes at higher energies in the spectrum that we do not attempt to interpret at this time. Importantly, the zero charge state spectrum (Figure 2, inset) is quantitatively restored (90 to 98%, data not shown) upon reduction of the Au_{38}^{1+} and Au_{38}^{2+} states back to Au_{38}^{0}. This ensures that the observed optical bleach is due to core-charging, not core degradation, and re-enforces the rationality of the model of Figure 3.

We must at this point remark on the obvious difference between the HOMO−LUMO gap energy (>1.3 eV) determined here for $Au_{38}(PhC_2S)_{24}$ and the 0.9 eV value previously reported by us and Whetten[3c] for alkanethiolate-coated 8 kDa MPCs and by Quinn.[8] The present $Au_{38}(PhC_2S)_{24}$ and previous 8 kDa samples are both well-characterized as to core size, at least as to be distinguishable from adjacent stable core dimensions (28, 55 atoms). It is possible that the difference in protecting ligands is a factor, although further investigation has not to date supported this thesis. Adsorbed bromide ligands on the level of one Br^- per MPC core or less cannot be cleanly ruled out, and this possible impurity in some of the samples we prepare is another concern. The energy gap observed here matches that[3b]

(19) (a) The UV−vis absorption spectrum of $Au_{38}(PhC_2S)_{24}$ is fitted to a sum of five Gaussians in Figure S-1 (Supporting Information). The fifth Gaussian at the highest energy (dashed line) is to take the UV rise in the absorption feature into account. (b) Shim, M.; Wang, C.; Guyot-Sionnest, P. *J. Phys. Chem. B* **2001**, *105*, 2369.

(20) Banin, U.; Cao, U.; Katz, D.; Millo, O. *Nature*, **1999**, *400*, 542.

(21) (a) Shim, M.; Guyot-Sionnest, P. *Nature* **2000**, *407*, 981. (b) Wang, C.; Shim, M.; Guyot-Sionnest, P. *Science* **2001**, *291*, 2390.

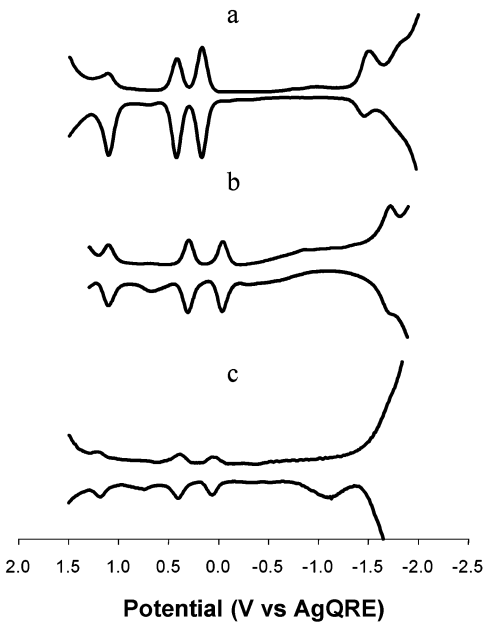

Figure 4. Differential pulse voltammograms (DPVs) at 25 °C and 20 mV/s of (a) $Au_{38}(PEG_{135}S)_{13}(PhC_2S)_{11}$, (b) $Au_{38}(C_6S)_{22}(PhC_2S)_2$, and (c) $Au_{38}(C_{10}S)_{19}(PhC_2S)_5$ in 0.1 M Bu_4NPF_6 in CH_2Cl_2 at 0.4 mm diameter Pt working, AgQRE, and Pt wire counter electrode.

of a glutathione-stabilized Au_{28} MPC, but we have no basis to question the analytical evidence supporting that formulation. We have no clear explanation for the difference between the presently and previously reported gap energies at this time.

Ligand-Exchanged Au_{38} MPCs. The Au_{38} core readily undergoes thiolate ligand place-exchange reactions, as shown previously in a study[18] in which a pegylated nanoparticle melt, $Au_{38}(PEG_{365}S)_{19}(PhC_2S)_5$ (PEG_{365} = a MW 365 thiolated poly(ethylene glycol)), was prepared from the $Au_{38}(PhC_2S)_{24}$ MPC. We have gone on to prepare other Au_{38} nanoparticles in a similar manner, as detailed elsewhere,[9,18] and describe here the electrochemical and spectral properties of the exchange products $Au_{38}(PEG_{135}S)_{13}(PhC_2S)_{11}$, $Au_{38}(C_6S)_{22}(PhC_2S)_2$, and $Au_{38}(C_{10}S)_{19}(PhC_2S)_5$.

DPV voltammetry of these mixed monolayer Au_{38} MPCs in CH_2Cl_2 at 25 °C, shown in Figure 4, is qualitatively similar to that of $Au_{38}(PhC_2S)_{24}$ in Figure 1. $Au_{38}(PEG_{135}S)_{13}(PhC_2S)_{11}$ and $Au_{38}(C_6S)_{22}(PhC_2S)_2$ show a doublet of oxidations (Figure 4a,b), a more positive oxidation step, and, like Figure 1, a first reduction widely separated from the first oxidation. These features appear, but less distinctly, in the DPV of $Au_{38}(C_{10}S)_{19}(PhC_2S)_5$ (Figure 4c), especially the reduction step which is only a weak shoulder at ca. −1.7 V. (The broad reoxidation peak at ca. −1.2 V is possibly due to degraded reduced product of this nanoparticle.) Data for the differences between the formal potentials of these reactions are given in Table 2 and for the actual potentials in Table S-2.

The electronic spectrum of the exchanged $Au_{38}(PEG_{135}S)_{13}(PhC_2S)_{11}$ MPC (Figure S-3) is, like the previously reported result[18] for $Au_{38}(PEG_{365}S)_{19}(PhC_2S)_5$, essentially identical to that of the parent $Au_{38}(PhC_2S)_{24}$ nanoparticle. This suggests that the Au_{38} core is substantially preserved during the PEG-thiolate exchange reactions. The spectral definition of the $Au_{38}(C_6S)_{22}(PhC_2S)_2$ sample was on the other hand degraded, showing a less detailed steplike structure (as if it were less monodisperse) and a greatly diminished absorption intensity around 700 nm.

Table 2. Formal Potential[a] Spacings (V) for Ligand Exchanged Au_{38} MPCs in CH_2Cl_2 Containing 0.1 M TBAP

MPC	*T* (°C)	ox3–ox2	ox2–ox1	ox1–re1
$Au_{38}(PEG_{135}S)_{13}(PhC_2S)_{11}$	25	0.68	0.26	1.65
$Au_{38}(PEG_{135}S)_{13}(PhC_2S)_{11}$	−70	0.68	0.19	1.69
$Au_{38}(C_6S)_{22}(PhC_2S)_2$	25	0.80	0.34	1.68
$Au_{38}(C_{10}S)_{19}(PhC_2S)_5$	25	0.80	0.34	
$Au_{38}(C_{10}S)_{19}(PhC_2S)_5$	−70	0.81	0.26	

[a] Formal potentials are averages of reduction and oxidation peak potentials in the DPV potential scans.

The $Au_{38}(C_6S)_{22}(PhC_2S)_2$ solution exhibited a rather positive electrochemical rest potential, indicating that the nanoparticle was in an oxidized state, which could account for the bleaching around 700 nm. Generally, Au_{38} cores with alkanethiolate ligands seem less stable than those with PhC_2S ligands.

Solvent Effects on Au_{38} MPC Properties. When a large molecule (or a molecule-like nanoparticle) is electrochemically oxidized or reduced, the observed electrochemical potentials are affected by the relative degrees of solvent dipole and electrolyte ion pairing stabilization of the electron donor and acceptor states. This effect is collectively called the "charging energy" and has been examined by many workers, including experiments on C60 in different solvents and electrolytes by Kadish et al.[22] and calculations[10] on 3.5 nm semiconductor nanoparticles bearing coatings of different dielectric constant but otherwise in a vacuum. Evans et al.[23] and Weaver et al.[24] have discussed, in different ways, the substantial effects of electrolyte/solvent media on charging energies attendant to reductions of organic molecules and C60, respectively. Charging energy normally enhances the energy difference between electrochemical oxidation and reduction potentials, relative to the optical band gap energy.

The effect of solvent polarity on the HOMO−LUMO gap and charging energies was examined by using 2:1 to 1:2 (v:v) mixtures of toluene and acetonitrile solvents (ϵ_S = 2.4 and 37, respectively). Voltammetry results at 25° and −40 °C for $Au_{38}(PhC_2S)_{24}$ MPCs (Figure 5, Table 1) show that the differences between formal potentials of the first oxidation and reduction steps, at both temperatures, decrease modestly (0.05 to 0.08 V) as the solvent mix becomes more polar. Table S-1 shows that while both $Au_{38}^{1+/0}$ and $Au_{38}^{0/1-}$ formal potentials shift positively in a more polar solvent environment, the latter shifts more; i.e., the reduced form of $Au_{38}(PhC_2S)_{24}$ is slightly stabilized relative to its oxidized form. The larger sensitivity of the $Au_{38}^{0/1-}$ reduction potential to the change in solvent may not of course be simply due to solvent polarity but may include other effects, for example, a stabilizing solvation of Au_{38}^- by the hydrophobic electrolyte cation.

The difference between the $Au_{38}^{+/0}$ (ox1) and $Au_{38}^{2+/+}$ (ox2) formal potentials was used above to estimate the charging energy contribution to the electrochemical energy gap. Table 1 shows that in 2:1 and 1:2 toluene/CH_3CN mixtures, this energy varies from 0.44 to 0.25 V and from 0.38 to 0.22 V at 25 and −40 °C, respectively. The analogous spacing between the $Au_{38}^{0/1-}$ (re1) and $Au_{38}^{1-/2-}$ (re2) formal potentials varies less, but in

(22) Dubois, D.; Moninot, G.; Kutner, W.; Jones, M. T.; Kadish, K. M. *J. Phys. Chem.* **1992**, *96*, 7137−7145
(23) Evans, D. H.; Hu, K. J. *Chem. Soc., Faraday Trans.* **1996**, *92*, 3983−3990.
(24) Roth, J. D.; Lewis, G. J.; Safford, L. K.; Jiang, X.; Dahl, L. F.; Weaver, M. J. *J. Am. Chem. Soc.* **1992**, *114*, 6159.

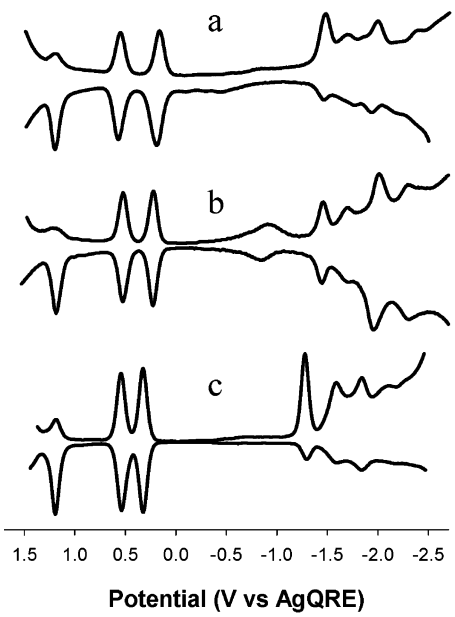

Figure 5. Differential pulse voltammograms (DPVs) at −40 °C and 20 mV/s of $Au_{38}(PhC_2S)_{24}$ in degassed 0.1 M Bu_4NPF_6 in (a) 2:1, (b) 1:1, and (c) 1:2 toluene/acetonitrile at 0.4 mm diam Pt working, AgQRE, and Pt wire counter electrode. The currents at ~ −0.8 V are due to residual oxygen that was not completely removed by the degassing.

the opposite direction. (Table S-1 shows the actual potentials and that the different formal potentials have decidedly different solvent sensitivities.) If one estimates charging energy from the difference between the $Au_{38}^{+/0}$ (ox1) and $Au_{38}^{2+/+}$ (ox2) formal potentials, over the range of solvents the electrochemically determined HOMO−LUMO gap energy varies from 1.24 to 1.35 eV; use of the analogous reductions to estimate charging energy gives gap energies of 1.44 to 1.30 eV. The message here is that our estimate of charging energy is quite rough but that most data indicate it as about 0.3 eV, and the corresponding electrochemical gap energy is about 1.3 eV as shown in Figure 3. The second message is that, as exemplified by studies by Kadish et al.,[22] multiple factors come into play in stabilization of differently charged molecule-like species in organic solvents, and an extremely detailed study is required to unravel the main ones.

We have previously[25] employed a concentric sphere capacitor model to estimate potential differences for quantized double layer charging of nanoparticles such as Au_{140} alkanethiolates. Single-electron changes in the capacitor charge occur at formal potentials spaced (ΔV) by

$$\Delta V = e/C_{CLU} = ed/4\pi\epsilon\epsilon_0 r(r + d) \qquad (1)$$

where e is electron charge, ϵ_0, the permittivity of free space, ϵ, the static dielectric constant of the monolayer medium around the metal core, r, the radius of the gold core, and d, the thickness of the monolayer medium. Smaller peak spacings are expected when the dielectric constant of the medium surrounding the metal core is higher. The model ignores the diffuse double layer.

Equation 1 is, in effect, a simple calculation of charging energy for nanoparticles, so it is worth comparing it to the Au_{38} data in Table 1, in particular to the differences in formal potentials of the $Au_{38}^{+/0}$ (ox1) and $Au_{38}^{2+/+}$ (ox2) couples of the $Au_{38}(PhC_2S)_{24}$ nanoparticles. In the case of alkanethiolate-protected Au_{140} MPCs, ΔV was roughly independent of the solvent medium.[25] For the Au_{38} MPCs, however, Table 1 shows that the solvent appears to make a difference. If the solvent dependency is expressed in terms of *effective* values of ϵ of the $Au_{38}(PhC_2S)_{24}$ MPC's monolayer, the Table 1 ox2−ox1 results would be satisfied by eq 1 using $r = 0.55$ and $d = 0.68$[25,26] by taking $\epsilon = 3.3$, 4.5, and 5.8 in the 2:1, 1:1, and 1:2 mixed toluene/acetonitrile solvents, respectively. When it is considered that toluene is probably strongly favored in the $Au_{38}(PhC_2S)_{24}$ solvation shell, these results are quite reasonable and suggest that the effective capacitance of the dielectric surrounding the Au_{38} core must be a combination of that of the ligand and of solvent that to some degree penetrates the ligand shell. The important conclusion is that the phenylethylthiolate monolayer ligand shell of the Au_{38} nanoparticle is somewhat open to intrusion by other species, which is geometrically unsurprising considering the sharp curvature of the Au_{38} surface.

The UV−vis spectra of $Au_{38}(PhC_2S)_{24}$ solutions on the other hand reveal no obvious solvent effects (Figure S-4). The spectra are essentially identical in CH_2Cl_2, toluene, and toluene/acetonitrile mixtures. Either the above-mentioned solvent intrusion is insufficient to provoke a measurable effect or the excited state nanoparticle is relatively nonpolar with a consequent weak dependence on the dielectric environment.

Photoluminescence of Au_{38} MPCs. The luminescence spectra of Au_{38} MPCs raise significant new issues in understanding these molecule-like nanoparticles. $Au_{38}(PhC_2S)_{24}$ nanoparticles luminescence only weakly, but that of ligand-exchanged versions is more intense and is illustrated by the Figure 6a emission spectra for $Au_{38}(PEG_{135}S)_{13}(PhC_2S)_{11}$. Spectra excited at 400 and 685 nm both show broad emission peaks around 1000 nm and can be fitted by two Gaussian-shaped emissions centered at 902 nm (1.38 eV) and 1025 nm (1.2 eV), shown as dashed lines. The excitation spectrum (inset, Figure 6a) shows that the emission intensity roughly follows the profile of absorbance (Figure 2), with the emission peak at 685 nm (1.8 eV) lying near the absorbance maximum at 670 nm. Figure 6b compares emission spectra taken at several different low-energy wavelength excitations: 600, 650, 680, and 750 nm. The emission differs substantially, being very weak when excited at 650 and 750 nm, being comparatively strong in both the 1.38 and 1.2 eV bands when excited at 680 nm, and favoring the higher energy component at 1.38 eV when excited at 600 nm. The sharply selective excitation behavior shows that emission from the higher energy channel (1.38 eV) is favored by higher energy excitation. It is also another indication of strongly condensed electronic energy levels.

The 1.38 eV emission from $Au_{38}(PEG_{135}S)_{13}(PhC_2S)_{11}$ nanoparticles matches very well the HOMO−LUMO gap energy determined above and can be assigned as relaxed luminescence across the HOMO−LUMO gap. On the other hand, the 1.2 eV band, which extends to energies as low as 0.89 eV (Figure 3), is obviously a sub-bandgap energy luminescence. The sub-gap emission energy is reminiscent of observations[3a] of emission energies (1.55 and 1.15 eV) from a glutathione-protected Au_{28} MPC, where the latter is lower than the optical absorbance edge energy (1.3 eV). The sub-gap emission was, in a solid-state-

(25) Hicks, J. F.; Templeton, A. C.; Chen, S.; Sheran, K. M.; Jasti, R.; Murray, R. W.; Debord, J.; Schaaff, T. G.; Whetten, R. L. *Anal. Chem.* **1999**, *71*, 3703.

(26) Wuelfing, W. P.; Murray, R. W. *J. Phys. Chem. B* **2002**, *106*, 3139.

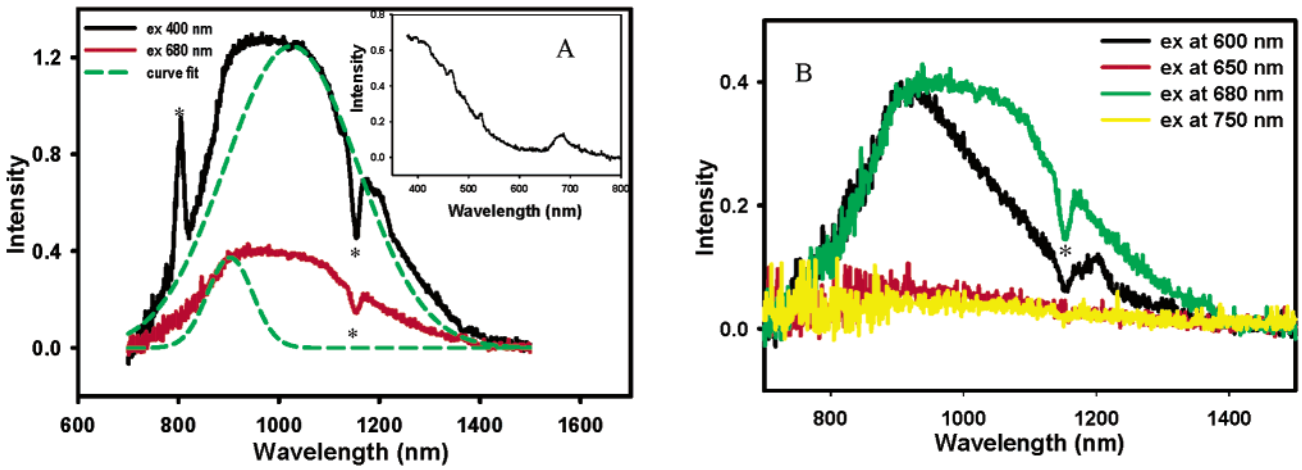

Figure 6. (a) Emission and excitation (inset) spectra of dilute $Au_{38}(PEG_{135}S)_{13}(PhC_2S)_{11}$ at 25 °C in CH_2Cl_2 (UV absorbance is 0.34 at 300 nm). Excitation and emission spectra were collected using $\lambda_{EM} = 1050$ nm and $\lambda_{EX} = 400$ and 680 nm, respectively. Dashed lines are Gaussian curvefits. Asterisks indicate artifacts from second-order excitation peak (800 nm) and solvent absorption (1165 nm). (b) Emission at indicated excitation wavelengths, λ_{EX}.

like analysis, ascribed to an intra-band transition and, in a molecular view, to emission from a possible triplet state. While that analysis is appealing, we have further observed,[27] and will report elsewhere that the near-IR emissions of Figure 6 can also be seen for a variety of Au MPCs of differing core dimensions and that they are very dependent on the ligands present. The overall picture is a complex one and probably must include dipole excitations that are associated with defect Au-ligand sites on the nanoparticle core surface.

Finally, we note the report by Yam et al.[3a,28] on the luminescence of Au(I) sulfido complexes. Recognizing that Au(I) thiolates are present in MPC solutions exposed to air,[13c,29] we examined solutions of Au(I) ligated to thiolates used here but observed no emission in the visible or near-infrared.

Acknowledgment. This research was supported in part by the STC Program of the National Science Foundation under Agreement No. CHE-9876674 and in part by grants from the U.S. Department of Energy, Division of Basic Sciences and the National Science Foundation. The authors gratefully acknowledge helpful discussions of this work with Dr. Stephen W. Feldberg, and R.L.D. thanks the Natural Sciences and Engineering Research Council of Canada for a postdoctoral fellowship.

Supporting Information Available: Synthesis of thiolated poly(ethylene glycol) ($PEG_{135}SH$) and DPV formal potentials for $Au_{38}(PhC_2S)_{24}$ in various solvents (Table S-1). This material is available free of charge via the Internet at http://pubs.acs.org.

JA049605B

(27) Wang, G.; Murray, R. W. Unpublished results, University of North Carolina−Chapel Hill, 2003.
(28) (a) Yam, V. W.-W.; Cheng, E. C.-C.; Zhou, Z.-Y. *Angew. Chem., Int. Ed.* **2000**, *39*, 1683. (b) Yam, V. W.-W.; Cheng, E. C.-C.; Cheung, K.-K. *Angew. Chem., Int. Ed.* **1999**, *38*, 197.
(29) Song, Y.; Huang, T.; Murray, R. W. *J. Am. Chem. Soc.* **2003**, *125*, 11694−11701.